Journal of Magnetic Resonance 202 (2010) 78–84

Contents lists available at ScienceDirect

Journal of Magnetic Resonance

journal homepage: www.elsevier.com/locate/jmr

Time-of-flight remote detection MRI of thermally modified wood

Ville-Veikko Telkki [a,*], Jani Saunavaara [a,b], Jukka Jokisaari [a]

[a] NMR Research Group, Department of Physics, University of Oulu, P.O. Box 3000, FIN-90014 Oulu, Finland
[b] Medical Imaging Centre of Southwest Finland, P.O. Box 52, FIN-20521 Turku, Finland

ARTICLE INFO

Article history:
Received 11 August 2009
Revised 2 October 2009
Available online 9 October 2009

Keywords:
NMR spectroscopy
Remote detection
Flow imaging
Wood
Thermal modification
Xenon

ABSTRACT

We demonstrate that time-of-flight (TOF) remote detection (RD) magnetic resonance imaging (MRI) provides detailed information about physical changes in wood due to thermal modification that is not available with conventional nuclear magnetic resonance (NMR) based techniques. In the experiments, xenon gas was forced to flow through *Pinus sylvestris* pine wood samples, and the flow paths and dispersion of gas atoms were observed by measuring ^{129}Xe TOF RD MRI images from the samples. MRI sensitivity of xenon was boosted by the spin exchange optical pumping (SEOP) method. Two different samples were studied: a reference sample, dried at low temperature, and a modified sample, which was thermally modified at 240 °C after the drying. The samples were taken next to each other from the same wood plank in order to ensure the comparability of the results. The most important conclusion is that both the smaller dispersion observed in all the TOF RD experiments independent of each other and the decreased amount of flow paths shown by the time projection of z-encoded TOF RD MRI experiment imply that a large amount of pits connecting tracheid cells are closed in thermal modification. Closed pits may be one reason for reduced moisture content and improved dimensional stability of wood achieved in thermal modification. This is the first time biological samples have been investigated by TOF RD MRI.

1. Introduction

Nuclear magnetic resonance (NMR) spectroscopy is one of the most versatile research methods applicable to investigations of, for instance, rotation, diffusion and flow phenomena of the molecules as well as molecular structures in liquid and solid states [1]. Its well-known application, magnetic resonance imaging (MRI), is a technique used in several disciplines, including medicine and material research, to visualize the structure of objects [2,3]. In the material research, direct NMR measurements of a solid material are often difficult, and the interpretation of the spectra is not easy matter due to large amount of broad lines. Furthermore, the relaxation time in solids is typically so short that the signal has decayed before detection if longer pulse sequences are applied. Hence, in many cases it is preferable to observe the NMR signal of a probe fluid absorbed in the material instead of that of the material, because the spectrum of probe fluid is simpler and its relaxation time is long. Spectra, relaxation times, pulsed-field-gradient spin-echo (PGSE) NMR based diffusion measurements, MRI and different flow imaging measurements of the probe fluid provide lots of information about structure, permeability and other properties of the material [4].

In many cases, the filling factor of the probe fluid inside the material is low leading to poor signal-to-noise ratio of NMR signal observed by a coil around the sample. Novel remote detection (RD) NMR technique [5] provides a solution to this problem. In the technique, the material is placed within the active volume of a relatively large coil (called encoding coil), and the spin coherences of a probe fluid flowing through the material are encoded with the coil. After that signal is detected in different spatial location with another, smaller detection coil with optimized filling factor (or alternatively with a more sensitive detector such as atomic magnetometer [6]). The flow of probe fluid transports the encoded spins to the detector. The encoding may cover all kind of NMR information. In the RD MRI experiment, the encoding step comprises the phase encoding, in which the positions of the probe molecules inside the encoding coil are encoded into spin coherences. The molecules encoded in different parts of the material arrive to the detector at different times. Consequently, RD MRI provides both time-of-flight (TOF) and spatial information about the fluid molecules as they flow from the encoding region to the detector, making it possible to obtain 3D TOF images of the fluid flow [7]. TOF RD MRI is a unique, non-destructive, and tracerless technique for determining flow paths and dispersion of fluid molecules in samples without optical access. So far, the method has been used to characterize porous media, rocks, and micro fluidic devices [5–10], and it has also been applied in relaxation measurements [11].

Here we demonstrate the potential of the TOF RD MRI technique in investigating biological systems, where fluid transport phenomena play a key role. We show that the technique provides lots of

* Corresponding author. Fax: +358 8 5531287.
E-mail address: ville-veikko.telkki@oulu.fi (V.-V. Telkki).

1090-7807/$ - see front matter © 2009 Elsevier Inc. All rights reserved.
doi:10.1016/j.jmr.2009.10.002

detailed information about changes in the structure of *Pinus sylvestris* pine wood due to thermal modification. Thermal modification is a relatively new method for increasing the lifetime and usability of timber products, and it has large commercial potential [12]. ThermoWood process developed in Technical Research Centre of Finland is a three phase process in which the intensive modification takes place at the temperature of about 200 °C for a few hours [13]. The modification improves the dimensional stability of wood, lowers its equilibrium moisture content, and increases its resistance to biodegradation and weather [12]. Contrary to many other wood treatment methods, thermal modification is pro-environmental, because only heat and water vapor are used in the process. The increased life time of timber products slows also down the greenhouse effect as atmospheric carbon dioxide is stored in the wood [12]. Thermally modified wood is used, for instance, in cladding, wall and ceiling panels, flooring, decking and garden and bathroom furnishing.

Xenon gas was used as a probe fluid, because the flow resistance of a gas is smaller than that of a liquid, and the sensitivity enhancement given by the spin exchange optical pumping (SEOP) method as well as the long T_1 relaxation time of ^{129}Xe make xenon a favorable gas for remote detection experiments [14]. In the SEOP method, circularly polarized laser light is first used to pump electronic spins of alkali metal vapor into population distributions far from equilibrium. Under suitable conditions polarization is then partially transferred from alkali metal valence electrons to noble gas nuclei in the pumping cell through spin-exchange collisions [15]. The most advanced hyperpolarizers can produce liter quantities of highly polarized (up to 70%) ^{129}Xe gas per hour [16].

Pinus sylvestris is comprised of three different cell structures (see Fig. 1): the portion of axial tracheids is 93.0 volume percent of the wood. Tracheids are boxlike in shape, and their average length (axial direction) and width (transverse direction) are about 2.8 mm and 25 μm, respectively. The hollow interior of tracheid cells is called the lumen. Radial rays containing a cylindrical cavity (diameter ~ 20 μm) comprise 6.4% of the wood. The portion of axial resin canals is 0.6%. Their cross-section is circular and their average diameter and length are about 80 μm and 50 cm, respectively [17].

Properties of wood have been studied with several different NMR techniques. PGSE NMR based diffusion measurements of liquids absorbed in wood have been used to determine the structure of wood [19–21]. This method mainly provides information about the dimensions of lumens inside tracheid cells in the transverse direction. Combined PGSE NMR of liquids and gases extends the range of observable dimensions from two to over four orders of magnitude, making it possible to also determine the axial dimensions of tracheids and the dimensions of the other cell structures [22]. However, previous studies have not revealed the connections between cells and cell structures, even though it is known that tracheid cells are connected to each other by small pits (see Fig. 1). In addition, PGSE NMR is not a very sensitive method for determining the properties of resin canals because of their small portion in wood, and, naturally, it does not give information about the spatial distribution of the canals. PGSE measurements of water absorbed in wood have also been applied for determining pore alignment [23]. The spatial heterogeneity of the porous structure of wood has been investigated by position exchange spectroscopy (POXSY) [24].

Chemical changes in wood at the molecular level caused by thermal modification have been studied using solid state NMR [25–28]. Observed changes in *P. sylvestris* are increased crystallinity of cellulose, increased lignin condensation, deacetylation of hemicelluloses, and demethoxylation of lignin, among others [25]. Changes in the porous structures formed by wood cells in the same wood species have been studied by means of PGSE NMR method [20]. The results have indicated that pore sizes increase when wood is treated at a high temperature.

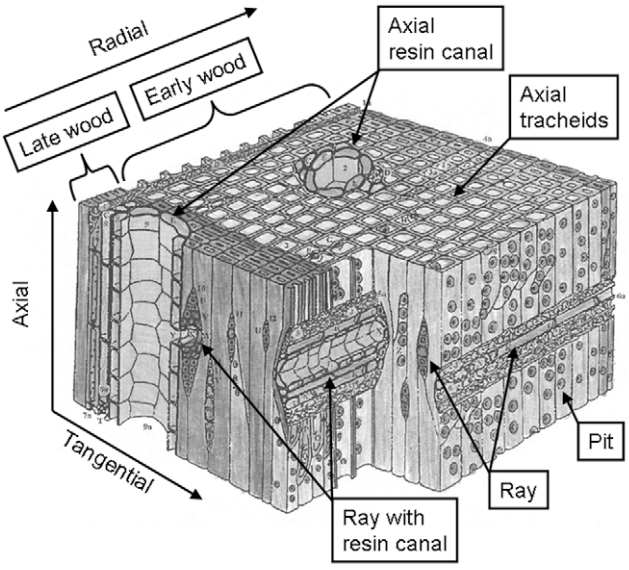

Fig. 1. Structure of *Pinus sylvestris* (modified after Kettunen [17] and Howard and Manwiller [18]).

2. Experimental

A *P. sylvestris* plank was first kiln-dried at a temperature of about 70 °C, and thereafter the plank was divided into two pieces. One part was used as untreated reference material, and the other part was thermally modified under steam using the ThermoWood process developed at VTT Building Technology, Finland [13]. The thermal modification process took 3 days, and the actual modification time at 240 °C was 4 h. A cylindrical sample was drilled with a plug drill from both modified and reference pieces from the locations next to each other in the original wood plank in order to ensure the comparability of the results. The pieces were relatively large (length 10 mm, diameter 8 mm) as compared to the microstructure of the wood and there were several annual rings in the samples. Therefore, a representative statistical average of the properties of the samples was observed in the experiments.

A cylindrical wood sample (axis parallel to the axial direction of the wood) was mounted inside a sample holder, which channeled probe fluid to flow through the sample (see Fig. 2). The height and diameter of the sample holder were 60 and 25 mm, respectively. Flow of probe fluid around the sample was prevented by wrapping a shrink wrap tightly around the sample. The empty spaces above and below the wood sample were filled with cotton to decrease the intensity of the signal observed from those regions.

The TOF RD MRI experiments were performed on a Bruker DSX300 spectrometer, where the resonance frequency of ^{129}Xe is 82.981 MHz. The encoding was done with a Bruker Micro 2.5 imaging probe using an rf insert with an inner diameter of 25 mm. The height of the encoding coil is 35 mm, and the sample was approximately in the center of the encoding coil region. The encoding probe body contained a 22 mm cylindrical cavity along its full length. A home-built detection probe was positioned into the imaging probe body so that the upper rim of the detection coil (saddle coil, height 10 mm, inner diameter 8 mm) was about 13 mm below the lower rim of the imaging coil, and the distance between the wood sample and the detection coil was about 3 cm (see Fig. 2). For more information about RD NMR detection probes, see Ref. [29]. A home-built, relay-based signal divider controlled by

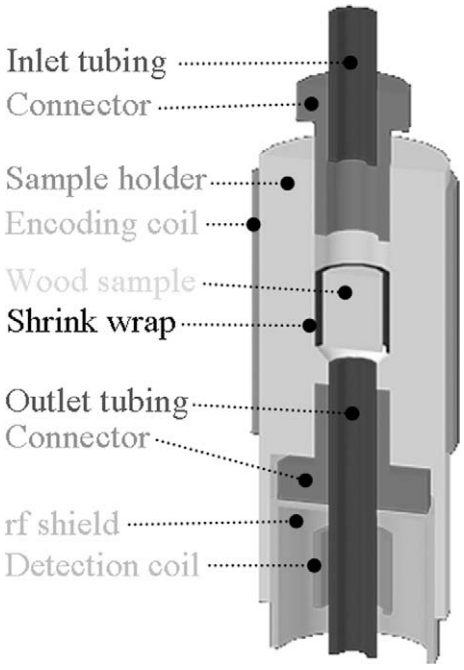

Fig. 2. Cross-section of the sample setup.

the trigger signal of the spectrometer was used to route the appropriate signals from the amplifier to both encoding and detection probes.

^{129}Xe nuclei were hyperpolarized using a home-built continuous flow system based on the design by Driehuys et al. [30]. A small amount (~0.5 g) of Rb was inserted directly inside a cylindrical polarization cell made of Pyrex glass (inner diameter 18 mm, length 120 mm). The cell was then placed inside an aluminum oven located between Helmholtz coils producing a homogeneous 13 G magnetic field. The beam of a 60 W Coherent Duo Fiber Array Packed (FAP) diode laser was directed into the polarization cell through a circular polarizer setup consisting of lenses, a linearly polarizing beam splitter cube, and a quarter-wave plate. A gas mixture consisting of helium (98%), nitrogen (1%), and xenon (1%) flew through the whole system and a pressure of 9 bar was maintained inside the polarization cell. Absorption of the laser light was monitored using an Ocean Optics USB2000 spectrometer, and the temperature inside the oven (~170 °C) was controlled to obtain ideal conditions for the SEOP process.

The flow rate of the gas mixture coming from the polarization cell was adjusted to be about 0.25 standard liters per minute (SLM). Eight percentage polarization of ^{129}Xe was routinely attained for this flow rate. Gas flow was monitored by a mass flow meter (Aalborg GFM17A) and controlled by a needle valve. The polarized gas mixture flowed through 1/4″ (6.35 mm) OD inlet tubing (ID 4 mm) to the sample holder, and similar outlet tubing led the gas from the holder through the detection coil to a vacuum pump (see Fig. 2). The gas pressure in the outlet tubing was kept around 1.5 bar. Because the pressure in the inlet tubing was estimated to be about 3 bar, an approximately 1.5 bar pressure difference between the ends of the wood sample produced the above-mentioned flow rate through the sample.

In all the remote detection experiments, the acquisition time of one free induction decay (FID) signal was 31 ms, which is also the time resolution in the TOF experiments. The acquisition time was set to be slightly shorter than the experimentally determined travel time of xenon gas through the detection coil. This ensured, on one hand, that we observed the signal of all the gas atoms, and, on the other hand, that the pulsing rate was slow enough relative to the travel time in order to prevent saturation of the signal. Consecutive FIDs (30–50) were collected during one scan, leading to a total acquisition time of 930–1550 ms per transient. The number of accumulated scans was four in the travel time experiments, whereas it was eight in all the other experiments. The experiment time in the travel time experiment was 9 s for the reference sample (30 FIDs) and 12 s for the thermally modified sample (50 FIDs). In all the RD MRI experiments, the length of the gradient pulse was 200 μs, and delay Δ (see Fig. 4a) was 300 μs (including the gradient pulse and gradient stabilization delay). The distance travelled and diffused by gas atoms during the gradient pulse was estimated to be shorter than 100 μm. As it is much smaller than the resolution in the images (see below), it did not cause any distortion in the images. In the *z*-encoded TOF experiments, the field of view (FOV) and resolution were 4 cm and 2.5 mm, respectively. Maximum gradient amplitude was 8.4 G/cm. The experiment time was 2 min 20 s for the reference sample (30 FIDs) and 3 min 47 s for the thermally modified sample (50 FIDs). In the *xz*-encoded TOF experiments, the FOV and resolution in the *z* direction were the same as in the *z*-encoded experiments, but only 1.2 cm and 1 mm in the *x* direction. Maximum gradient amplitudes in *x* and *z* directions were 21.1 G/cm and 8.4 G/cm, respectively. The experiment time was 27 min for the reference sample (30 FIDs) and 36 min for the thermally modified sample (40 FIDs). In the *xy*-encoded experiments, the FOV and resolution were 1.2 cm and 1 mm in both directions, and maximum gradient amplitudes were 21.1 G/cm. The experiment time was 20 min for the reference sample (30 FIDs) and 27 min for the thermally modified sample (40 FIDs).

3. Results and discussion

3.1. Travel time experiments

The pulse sequence of the RD NMR travel time experiment [5] and the travel time curves measured from the reference and thermally modified samples are shown in Fig. 3. In the travel time experiment, the spins inside the encoding coil are first inverted by applying a π pulse, and then the magnetization of the spins flowing into the detection coil is read by a train of $\pi/2$ pulses. Hence, the decrease in the amplitude of the observed signal indicates when the inverted spins from the encoding coil region arrive in the detector.

First, the spins below the encoding coil region that have not experienced the inversion pulse arrive in the detector, and a large, positive signal is observed. The amplitude of the signal was normalized to be 1 in Fig. 3. Later, as the time *t* between the inversion pulse and detection increases, the inverted spins arrive in the detector, decreasing the observed signal amplitude. However, a fully inverted signal (amplitude – 1) was not observed, because, due to dispersion, the inverted spins are always mixed with the non-inverted spins. T_1 relaxation may also prevent observation of a perfect inversion. However, the effect of relaxation is small because T_1 of xenon is long (on the order of a minute) when compared with the travel times (shorter than a second). (The relaxation time of xenon absorbed in wood is long because the size of pores in wood is large, on the order of tens of micrometers, and, contrary to many inorganic porous materials, there is no paramagnetic center in wood.) Furthermore, degrease of driving pressure during the experiment may also prevent an observation of perfect inversion. However, the observed pressure decrease was less than 0.2% during the travel time experiment. Therefore, its effect is negligible. When *t* is large enough, the non-inverted spins above the encoding coil arrive in the detector and the amplitude of the signal approaches a value of 1.

The travel time curve of the thermally modified sample approaches the minimum faster than that of the reference sample.

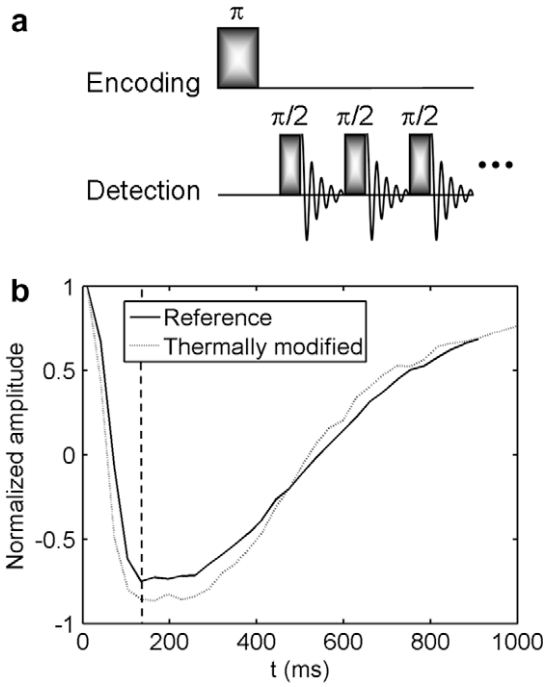

Fig. 3. (a) Pulse sequence of the travel time experiment. (b) Travel time curves measured from the reference and thermally modified samples. The vertical dashed line shows the time instant when the first spins inverted inside the wood samples arrive in the detector (deduced from the TOF RD MRI images shown later).

This may be a consequence of the slightly larger flow rate in the former case. The minimum is deeper in the case of the modified sample, which implies that the dispersion is slightly greater in the reference sample.

3.2. z-encoded TOF experiments

The pulse sequence of z-encoded TOF RD MRI experiment [7] is shown in Fig. 4a. The experiment begins with a $\pi/2$ pulse, and thereafter the positions of the atoms inside the encoding coil are encoded into spin coherences by a magnetic field gradient pulse. Next, the coherences are stored as a longitudinal magnetization in order to prevent dephasing during the flow to the detector. Finally, the amplitude of the encoded magnetization is read by a train of $\pi/2$ pulses in the detection coil. The resulting image shows the z position distribution of the atoms, which arrive in the detector at time t, during the encoding.

The results of the z-encoded TOF experiments are shown in Figs. 4b and c. Three different regions can be seen in the images: the outlet region below $z \sim 1.7$ cm, the sample region at $z \sim 1.7$–2.7 cm, and the inlet region above $z \sim 2.7$ cm (see also Fig. 2). The amplitude in the sample region is low because wood is dense. The images show that the gas atoms from the outlet region arrive in the detector first, then the atoms from the sample region, and finally the atoms from the inlet region. The "slopes" of the z-encoded TOF images reveal the average flow velocity in the different regions. We determined the maximum of the signal amplitude in the z direction as a function of t, and, using this data, we calculated that the average flow velocity in the outlet region was about 17 cm/s for both samples. The "slope" in the sample regions is infinite, which means that the travel time of some of the gas atoms through the sample is shorter than the time resolution in the experiment (31 ms). (On the other hand, broadening of signal region in t direction shows that there is a large distribution of travel times of molecules through the wood sample, see dispersion analysis below.) Hence, we conclude that the average flow velocity in the sample regions was greater than 35 cm/s. The average flow velocity in the inlet region was about 1.1 cm/s.

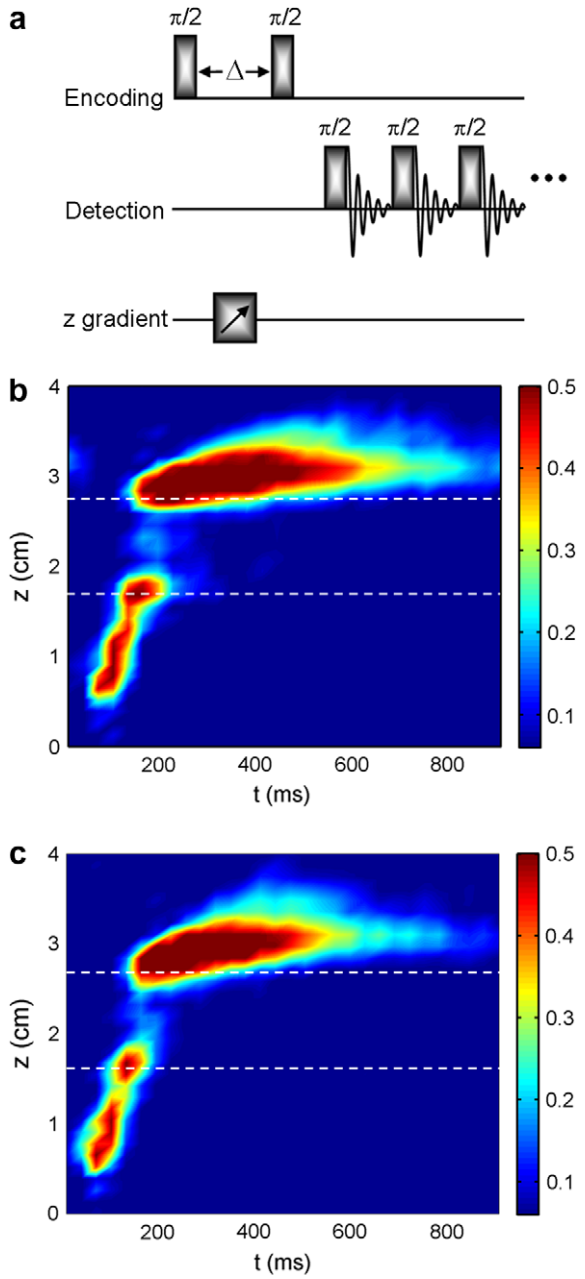

Fig. 4. Pulse sequence of the z-encoded TOF experiment (a), and z-encoded TOF images measured from (b) the reference and (c) thermally modified samples. The sample regions are indicated by dashed lines in the images.

The amplitudes of MRI images in different z regions reflect the total volume of flow paths in the regions. The sum of the amplitudes measured at different travel time instants as a function of z (z time projection) is shown in Fig. 5. The amplitude, $a(z)$, is proportional to the product of gas pressure, $P(z)$, and the total volume of the flow paths, $V_p(z)$:

$$a(z) \propto P(z)V_p(z) = P(z)A_p(z)\Delta z \quad (1)$$

Here, $A_p(z)$ is the total area of the cross-sections of the flow paths, and Δz is the resolution in the z direction. Because Δz is a constant, we obtain

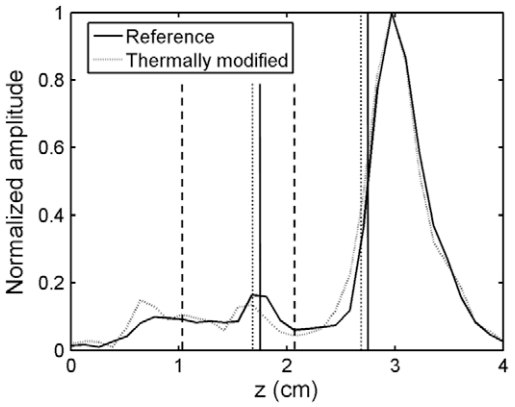

Fig. 5. z time projection, where the maximum amplitude around $z = 3$ cm was normalized to be 1. The reference and thermally modified sample regions are shown with vertical solid and dotted dashed lines, respectively. The right vertical dashed line shows the amplitudes in the center of the sample region that are proportional to A_p, whereas the left dashed line shows the amplitudes in the outlet tubing that are proportional to A_s. These values were used in the calculation of the percentage flow paths by Eq. (3).

$$\frac{a(z)}{P(z)A_p(z)} = \text{constant} \tag{2}$$

The constant can be calculated because a, P, and, A_p in the outlet tubing are known (see Fig. 5 and Section 2). In the sample region, a is also known (see Fig. 5) and the gas pressure is between 1.5 and 3 bar, which are the pressures in the outlet and inlet tubing, respectively. Hence, it is possible to estimate the value of A_p in the wood sample. The percentage of flow paths, p_p, in the wood sample is

$$p_p = \frac{A_p}{A_s} \cdot 100\% \tag{3}$$

Here, A_s is the area of the cross-section of the sample. Consequently, we calculated that p_p in the reference sample is 8.2–16%, whereas it is 5.0–10% in the thermally modified sample, depending on the gas pressure in the sample.

Axial resin canals that go all the way through the wood sample (see Fig. 1) were thought to be natural flow paths for the gas. However, their relative portion in *P. sylvestris* is only 0.6%, and therefore the above p_p values show that a large amount of gas flows through longitudinal tracheids, which are the only possible flow paths besides resin canals. Because the average length of tracheids is about 2.8 mm, the gas atoms pass several tracheid cells connected by small pits as they flow through the sample (10 mm in length). It has been observed that the pits are closed when wood is heated above 100 °C [17], and this may restrict gas from flowing through tracheid cell network. The smaller p_p of the thermally modified sample may be a consequence of this phenomenon. However, the measured p_p in the thermally modified sample is still substantially larger than the portion of resin canals, indicating that either all the pits are not entirely closed or the wood cell structure is partially destroyed because of the treatment (as it is suggested in Ref. [20]), allowing the gas to flow more freely through the tracheid cell network.

From Figs. 4b and c, one gets the impression that the signal spreads wider along in the t direction in the reference sample region than in the thermally modified sample region, meaning that the dispersion of gas is slightly greater in the former case. This can be shown quantitatively by determining the full widths at half maxima of the signals (denoted by Δt) as a function of z (see Fig. 6). Below $z \sim 1.7$ cm, Δt increases slowly and equally in both experiments with increasing z because of small dispersion in the outlet

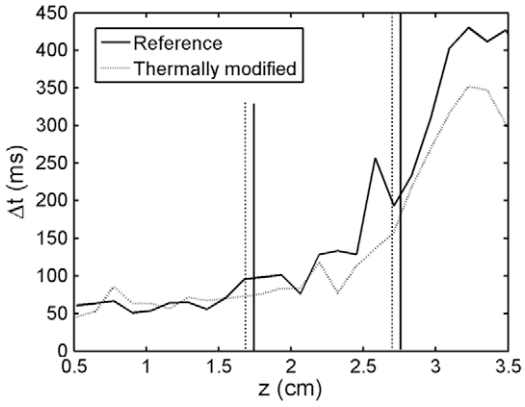

Fig. 6. Dispersion as a function of z. Δt is the full width at half maximum of the z-encoded TOF curve. The reference and thermally modified sample regions are shown with vertical solid and dotted dashed lines, respectively.

region. The increased slope at $z \sim 1.7$–2.7 cm shows that dispersion in the sample region is larger than in the outlet region. Furthermore, the curves show that the dispersion is larger in the reference sample than in the modified sample, because Δt values of the reference sample are higher. The values of Δt in the reference sample are also higher in the inlet region (above $z \sim 2.7$ cm) because of cumulative appearance of dispersion in the curves (the atoms encoded in the inlet region flow through the wood sample before detection).

The travel time experiments also support the observation of larger dispersion in the reference sample (see Section 3.1). Small pits connecting the tracheid cells cause large dispersion of gas flowing through tracheid cell network. Consequently, the dispersion of gas flowing through tracheid cell network is greater than that of gas flowing through relatively large, straight resin canals. Analysis of z time projections showed that the relative amount of gas flowing through tracheid cells is greater in the case of the reference sample than in the case of the modified sample (see above), and therefore the dispersion is greater in the reference sample than in the modified sample.

3.3. *xz*- and *xy*-encoded TOF experiments

The pulse sequences of *xz*- and *xy*-encoded TOF RD MRI experiments are otherwise identical with z-encoded TOF experiment shown in Fig. 4a, but the gradient pulses are applied in x and z directions in the former case and in x and y directions in the latter case. Therefore, the experiments reveal what was the position distribution of the molecules, which arrive into the detector at t, in *xz* or *xy* plane during the encoding. The results are shown in Fig. 7.

There are several indications in the $t = 41$–134 ms images that the flow in the outlet tubing is laminar: the $t = 41$ ms images show that the atoms in the center of the tubing on the bottom of the encoding coil region arrive in the detector first, whereas the low amplitude in the center of the *xy* images measured at $t = 72$ ms reveals that the atoms close to the walls of the tubing arrive in the detector later than those in the center of the tubing. Furthermore, a parabolic flow profile is seen in the *xz* images measured at $t = 134$ ms, which is one more proof of laminar flow. We estimated that the Reynolds number in the outlet tubing is about 20, evidencing that the flow is really laminar. In addition, the diffusion time of xenon across the tubing (diameter $d = 4$ mm) is $d^2/2D = 1.5$ s (diffusion coefficient of xenon gas is $D = 5.3 * 10^{-6}$ m^2/s [31]), which is much longer than the travel time of the atoms from the outlet tubing to the detector. Consequently, transverse diffusion does not

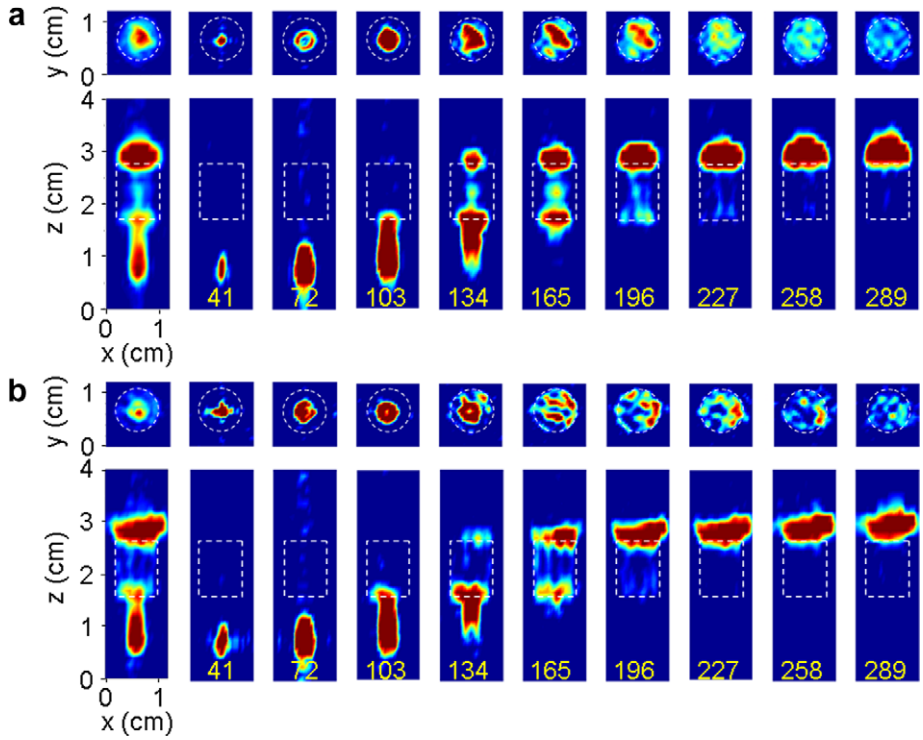

Fig. 7. Selected *xy*- (upper) and *xz*- (lower) encoded TOF images measured from (a) the reference and (b) thermally modified samples. The travel time instances in milliseconds are shown in the images. Images on the left are the sum of the images measured at $t = 41–289$ ms. The sample regions are indicated by dashed lines in the images.

average the travel times and a flow profile typical of laminar flow is observed from the outlet tubing.

In the $t = 134$ ms images, signals from the outlet, sample and inlet regions are seen, showing again (see also Section 3.2) that some of the atoms travel faster through the wood sample than what is the time resolution in the experiments (31 ms). Strong, tilted stripes are seen in the *xy* images measured from both samples at $t = 165$ ms. By comparing the orientation of the samples with the frame of reference of the gradient system, we observed that the annual rings were parallel to the stripes and early wood regions were in the same position as the stripes. Therefore, we conclude that gas flowed mainly through early wood. This is reasonable, because late wood is denser than early wood. The signal from the sample region is still seen in the *xz* image measured from the reference sample at $t = 227$ ms, whereas it has disappeared from the corresponding image measured from the thermally modified sample. This confirms the conclusion stated earlier (Sections 3.1 and 3.2), that the dispersion of gas is greater in the reference sample than in the modified sample.

The *xy* images are patchy at the longest TOF instances shown in Fig. 7 because the signal arises from the inlet region, which is filled with cotton, whose density is not constant.

4. Conclusions

This work evidences that TOF RD MRI can provide detailed information about biological samples. Specifically, it elucidates how thermal modification changes the properties of *P. sylvestris* pine wood. The images show that the percentage of flow paths in the unmodified reference sample is greater than in the thermally modified sample and that a substantial amount of gas flows through tracheid cell network. Flow through tracheid cell network is lower in the thermally modified sample, implying that a large amount of the pits connecting the cells are closed during the modification. All the TOF RD experiments independent of each other revealed decreased dispersion in the modified sample. We deduced that the dispersion of gas was greater in the reference sample, because the relative amount of gas flowing through tracheid cells instead of resin canals is greater than in the thermally modified sample and the dispersion of gas in tracheid cell network is larger than in resin canals. Hence, the dispersion analysis evidences also that some of the pits connecting the cells are closed during the modification. The observed closing of the pits in the modification may play an important role in achieving such desired properties in thermal modification as reduced moisture content and improved dimensional stability. As the connections between tracheid cells could not be observed with PGSE NMR based methods in previous studies [19–22], TOF RD MRI increases crucially information given by NMR methods in wood research. The images also reveal that most of the gas flowed through early wood in both samples. These proof-of-principle experiments show that TOF RD MRI provides essential information about the physical changes in wood in thermal modification. An extensive investigation of wood samples modified in different temperatures by this technique will follow later. The experimental setup will be slightly modified in order to increase the precision of the measurements: For instance, the volume of gas inside the detection coil will be decreased in order to increase the time resolution in the experiment. This enables more precise determination of fluid dispersion in wood. In addition, the empty volumes above and below wood sample will be made smaller in order to decrease the signal amplitude and dispersion in these regions. This is also the first time biological samples have been investigated by TOF remote detection MRI.

Acknowledgments

This work was supported by the Academy of Finland (Grants No. 123847 and 116824), The Finnish Cultural Foundation and the

Instrumentarium Science Foundation. We thank Jorma Mäkitalo, Tapani Mäntykenttä, and Erkki Laukkanen from the machine shop of the Department of Physics for preparing the detection probe, sample holder and signal divider, as well as for help in building the xenon hyperpolarizer, Jyrki Ruohonen for his contribution to the planning of the hyperpolarizer, NMR Facility Manager Anu Kantola for help in experimental issues, and professor Sirkka-Liisa Maunu for providing us the wood samples.

References

[1] M.H. Levitt, Spin Dynamics: Basics of Nuclear Magnetic Resonance, Wiley, Chichester, 2001.
[2] E.M. Haacke, R.W. Brown, M.R. Thompson, R. Venkatesan, Magnetic Resonance Imaging, Wiley, New York, 1999.
[3] B. Blümich, NMR Imaging of Materials, Oxford University Press, Oxford, 2000.
[4] P.T. Callaghan, Principles of Nuclear Magnetic Resonance Microscopy, Clarendon Press, Oxford, 1991.
[5] A.J. Moule, M. Spence, S. Han, J. Seeley, K. Pierce, S. Saxena, A. Pines, Amplification of xenon NMR and MRI by remote detection, Proc. Natl. Acad. Sci. USA 100 (2003) 9122–9127.
[6] S. Xu, V.V. Yashchuk, M.H. Donaldson, S.M. Rochester, D. Budker, A. Pines, Magnetic resonance imaging with an optical atomic magnetometer, Proc. Natl. Acad. Sci. USA 103 (2006) 12668–12671.
[7] J. Granwehr, E. Harel, S. Han, S. Garcia, A. Pines, Time-of-flight flow imaging using NMR remote detection, Phys. Rev. Lett. 95 (2005) 075503.
[8] E. Harel, J. Granwehr, J. Seeley, A. Pines, Multiphase imaging of gas flow in a nanoporous material using remote-detection NMR, Nat. Mater. 5 (2006) 321–327.
[9] C. Hilty, E. McDonnell, J. Granwehr, K. Pierce, S. Han, A. Pines, Microfluidic gas-flow profiling using remote-detection NMR, Proc. Natl. Acad. Sci. USA 102 (2005) 14960–14963.
[10] V.-V. Telkki, C. Hilty, S. Garcia, E. Harel, A. Pines, Quantifying the diffusion of a fluid through membranes by double phase encoded remote detection magnetic resonance imaging, J. Phys. Chem. B 111 (2007) 13929–13936.
[11] Z.I. Cleveland, G.E. Pavlovskaya, K.F. Stupic, C.F. LeNoir, T. Meersmann, Exploring hyperpolarized ^{83}Kr by remotely detected NMR relaxometry, J. Chem. Phys. 124 (2006) 044312.
[12] C.A.S. Hill, Wood Modification, Wiley, Chichester, 2006.
[13] P. Viitaniemi, S. Jämsä, P. Ek, H. Viitanen, Pat. US-5678324: Method for improving biodegradation resistance and dimensional stability of cellulosic products.
[14] B.M. Goodson, Nuclear magnetic resonance of laser-polarized noble gases in molecules, materials, and organisms, J. Magn. Reson. 155 (2002) 157–216.
[15] T.G. Walker, W. Happer, Spin-exchange optical pumping of noble-gas nuclei, Rev. Mod. Phys. 69 (1997) 629–642.
[16] I.C. Ruset, S. Ketel, F.W. Hersman, Optical pumping system design for large production of hyperpolarized ^{129}Xe, Phys. Rev. Lett. 96 (2006) 053002.
[17] P.O. Kettunen, Wood: Structure and Properties, Trans. Tech. Publications, Zürich, 2006.
[18] E.T. Howard, F.G. Manwiller, Anatomical characteristics of southern pine stemwood, Wood Sci. 2 (1969) 77–86.
[19] W. Wycoff, S. Pickup, B. Cutter, W. Miller, T.C. Wong, The determination of the cell size in wood by nuclear magnetic resonance diffusion techniques, Wood Fiber Sci. 32 (2000) 72–80.
[20] S. Hietala, S.L. Maunu, F. Sundholm, S. Jämsä, P. Viitaniemi, Structure of thermally modified wood studied by liquid state NMR measurements, Holzforschung 56 (2002) 522–528.
[21] E.H. Johannessen, E.W. Hansen, J.B. Rosenholm, Fluid self-diffusion in Scots pine sapwood tracheid cells, J. Phys. Chem. B 110 (2006) 2427–2434.
[22] P. Kekkonen, V.-V. Telkki, J. Jokisaari, Determining the highly anisotropic cell structures of *Pinus sylvestris* in three orthogonal directions by PGSTE NMR of absorbed water and methane, J. Phys. Chem. B 113 (2009) 1080–1084.
[23] R. Meder, S.L. Codd, R.A. Franich, P.T. Callaghan, J.M. Pope, Observation of anisotropic water movement in *Pinus radiata* D. Don sapwood above fiber saturation using magnetic resonance micro-imaging, Holz. Roh. Werkst. 61 (2003) 251–256.
[24] V.-V. Telkki, J. Jokisaari, Determination of the structure of wood from the self-diffusion probability densities of a fluid observed by position-exchange NMR spectroscopy, Phys. Chem. Chem. Phys. 11 (2009) 1167–1172.
[25] S.L. Maunu, NMR studies of wood and wood products, Prog. Nucl. Mag. Res. Sp. 40 (2002) 151–174.
[26] B. Tjeerdsma, M. Boonstra, A. Pizzi, P. Tekely, H. Militz, Characterisation of thermally modified wood: molecular reasons for wood performance improvement, H. Holz Roh. Werkst. 56 (1998) 149–153.
[27] B. Kosiková, M. Hricovíni, C. Cosentino, Interaction of lignin and polysaccharides in beech wood (*Fagus sylvatica*) during drying processes, Wood Sci. Technol. 33 (1999) 373–380.
[28] H. Sivonen, S.L. Maunu, F. Sundholm, S. Jämsä, P. Viitaniemi, Magnetic resonance studies of thermally modified wood, Holzforschung 56 (2002) 648–654.
[29] S. Han, J. Granwehr, S. Garcia, E.E. McDonnell, A. Pines, Auxiliary probe design adaptable to existing probes for remote detection NMR, MRI, and time-of-flight tracing, J. Magn. Reson. 182 (2006) 260–272.
[30] B. Driehuys, G.D. Cates, E. Miron, K. Sauer, D.K. Walter, W. Happer, High-volume production of laser-polarized ^{129}Xe, Appl. Phys. Lett. 69 (1996) 1668–1670.
[31] M. Pfeffer, O. Lutz, ^{129}Xe gas NMR spectroscopy and imaging with a whole-body imager, J. Magn. Reson. Ser. A 108 (1994) 106–109.